2020 IEEE/RSJ International Conference on Intelligent Robots and Systems (IROS)
October 25-29, 2020, Las Vegas, NV, USA (Virtual)

Development of a Running Hexapod Robot with Differentiated Front and Hind Leg Morphology and Functionality

Jia-Ruei Chiu, Yu-Chih Huang, Hui-Ching Chen, Kuan-Yu Tseng, and Pei-Chun Lin

Abstract— **This article introduces an innovative model-based strategy for designing a legged robot to generate animal-like running dynamics with differentiated leg braking and thrusting force patterns. Linear springs were utilized as legs, but instead of having one end of each spring connected directly to the hip joint, one extra bar was added to offset the spring's direction. The robot's front and hind legs were offset with the same magnitudes but in different directions. Therefore, the legs produced different ground braking and thrusting force patterns. The robot's running motion was planned based on its reduced-order model. The model's fixed-point and passive-dynamics motion served as the robot's reference motion. The proposed strategy was experimentally validated, and the results confirmed that the robot could successfully perform stable running in a differentiated leg force pattern.**

I. Introduction

Throughout millions of years, legged animals have evolved intricate morphologies, high degrees of freedom (DOF), and prominent sensing and maneuvering ability, which have enabled them to move with unrivaled agility and mobility on various terrains. The underlying mechanism of the locomotion and dynamics animals use in their complex structures is difficult to study. Nevertheless, the running motions of various legged animals can be closely imitated by the reduced-order and single-leg spring-loaded inverted pendulum (SLIP) model [1], [2], which is composed of a point mass as the body and a massless linear spring as the leg, despite the fact that the morphology and number of legs differ greatly among legged animals. Furthermore, the SLIP model can be regarded as the template to represent and control the animal with complex and redundant morphology as the anchor [3].

In addition to the SLIP model, a variety of reduced-order templates have been proposed, which focus mainly on changes in morphology and energy flow. In the SLIP-R model, a rolling foot was added to the SLIP model to increase dynamics and performance [4]. In the torqued-damped SLIP (TD-SLIP) and clock-torqued SLIP (CT-SLIP) models, hip torque/damping and hip position control are embedded for better matching to realistic situations [5]–[7]. The asymmetric SLIP (ASLIP) was proposed to model the monopod hopper, in which the hip joint and the center of mass (COM) are not coincident [8]. Previously, we proposed several reduced-order models with special attention to their utilization in initiating the dynamic behaviors of the robot. The conservative rolling SLIP (R-SLIP) model with a large rolling foot enabled the RHex [9]-style robot to run at various speeds [10]. Its successor, the clock-torqued R-SLIP (CTR-SLIP) model, which took into account robot leg control, further enabled the robot to switch running speeds in situ [11]. Another study on the torque-actuated dissipative R-SLIP (TDR-SLIP) model investigated the leg design and its mechanical properties on the dynamic behaviors of a robot [12]. The SLIP model was utilized as the template to initiate dynamic running in a leg-wheel transformable robot as well [13], [14]. The reduced-order models were mainly utilized as the template for abstracting overall robot dynamics. Thus, for a legged robot that utilized a gait with multiple ground-contact legs, such as the tripod gait, the effects of individual legs were summarized as one virtual leg, and the functionality difference among individual legs was ignored.

The research in animal locomotion shows that the legs of animals have different functions. For example, the cockroach's front legs serve as a decelerator and a body-lifter to keep it running stably [15]. The stick insect's hind leg supports the body weight and thrusts the body forward while its middle and front legs have support and feeler functions, respectively [16]. When the gecko decelerates or accelerates, it stabilizes its body pitch by decelerating its front legs or thrusting its hind legs, respectively [17]. In addition to biologists, a few robotics researchers also explored the leg functionality differentiation problem. The Minitaur [18] had identical legs, and it performed different leg functions by adjusting the touchdown and swing angles of the legs [19]. The front and hind legs of the MIT Cheetah are designed differently to mimic this animal's morphology. The hind legs are capable of performing strong thrusts during fast running [20]. The front, middle, and hind legs of the hexapod Sprawl family [21]–[23] of robots have identical morphology, but the legs are configured in different orientations to differentiate their ground interaction forces. The individual leg motions of the reported works were designed separately without using the abstract model.

Here, we report an innovative model-based strategy for use in designing a legged robot to generate animal-like running dynamics with differentiated leg braking and thrusting force patterns. The linear spring was utilized for the legs owing to its easy adaptation to the template and anchor theme [3]. Instead of connecting one end of the spring to the hip joint, one extra bar was added to offset the spring's direction. The robot's front and hind legs were offset with

This work is supported by the Ministry of Science and Technology (MoST), Taiwan, under contract: MOST 107-2634-F-002-004-.

The authors are with the Department of Mechanical Engineering, National Taiwan University, No. 1 Roosevelt Rd. Sec. 4, Taipei, Taiwan. (Corresponding author: Pei-Chun Lin: phone: +886-2-3366-9747; fax: +886-2-3366-9914; email: peichunlin@ntu.edu.tw).

the same magnitudes but in different directions. Therefore, the SLIP-like legs could produce different ground braking and thrusting force patterns, as the analysis shows. The robot's running motion was planned based on this SLIP-like reduced-order model. The model's fixed-point and passive-dynamics motion served as the robot's reference motion. The proposed strategy was experimentally validated in the present study. In short, the design and control of the robot were inspired mainly by the morphology and dynamics of a simple reduced-order model, where its two variations (i.e., offsets) were individually mapped to the robot's front and hind legs. Thus, compared to the reported template and anchor theme, which only concerns body dynamics, this work extended the use of the reduced-order model to simultaneously consider the individual leg's functionality. To the best of our knowledge, this is the first work to achieve a robot running with leg function differentiated simultaneously, which differs in both leg morphology design and robot control approaches based on the simple one-leg reduced-order model. The process does not involve rigid-body dynamics or any parameter tuning and optimization.

The remainder of this article is organized as follows: Section II introduces the leg model. Section III describes the design of the robot leg and the plan of the robot motion based on the model. Section IV reports the experimental results, and Section V concludes the work.

II. Development of the Leg Model

A. Design concept

The use of passive springs for the robot's legs was based on the following reasons: (i) The morphology was feasible to be mapped to the template and anchor theme, so the design of the robot's behavior could be achieved. Previously, we utilized the R-SLIP model as the running template to initiate running of an RHex-style robot at various speeds [10]. In that work, the robot's tripods were alternatively mapped to the virtual leg of the R-SLIP model. (ii) It was feasible to analyze the dynamics of the leg in this morphology, so the tools of nonlinear dynamics, such as the Poincaré Return Map and fixed points, could be utilized. When the robot ran horizontally, the body inertia had no effect. In this case, the robot's body could be approximated by point mass, so the motion could be analyzed in the reduced-order form. (iii) The differentiation in morphology and functionality could be achieved by simply adding an offset, and this offset generated differentiation in force functionality. (iv) Following (iii), this offset had only a minor effect on the motion states of the point mass. Thus, when the robot utilized its front and hind legs with different offsets, the robot's leg motions could still be planned separately using two point-mass models (i.e., only one model with two offsets) without involving rigid body dynamics.

The leg can be modeled as the evolved version of the traditional SLIP model. The SLIP model is a reduced-order, conservative, and one-legged model that approximates the running motion of legged animals in the sagittal plane. The model is parametrized by three intrinsic parameters,

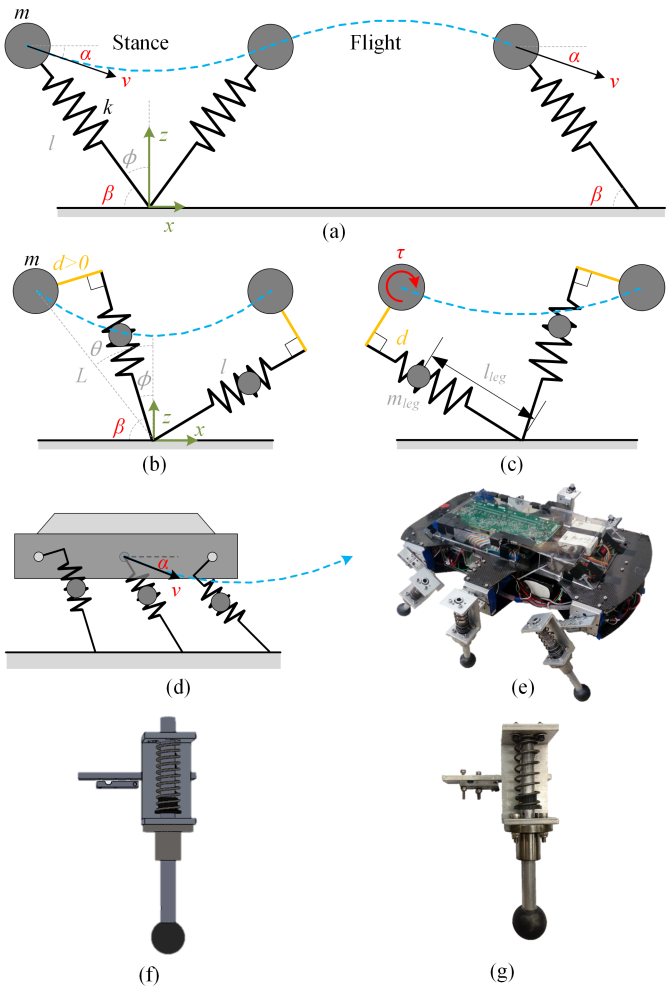

Fig. 1. The models and the robot: (a) the SLIP model; (b) and (c) the eSLIP models with positive and negative offset, respectively; (d) and (e) the CAD drawing and the photo of the robot that uses eSLIP legs with different offsets; (f) and (g) the CAD and the photo of the robot leg that realizes the eSLIP leg

including point mass (m), leg length (l), and spring stiffness (k), as shown in Fig. 1(a). In other words, the upper body of the legged animal is abstractly approximated by a point mass, and the leg in stance is approximated by a massless and linear spring. The SLIP model can perform a stable running motion (i.e., with alternative stance and flight motion) if it begins the stance phase in an adequate touchdown state, which includes touchdown speed (v), touchdown angle (α), and landing angle (β), as shown in Fig. 1(a). During the stance phase, the kinetic, spring potential, and gravitational potential energies of the model are exchanged, and the model first decelerates and then accelerates.

With the aim of using the SLIP-like model as the running template of the multi-legged system as well as providing differentiated leg functionality, the leg model has the following variations with respect to the SLIP model:

(i) The model has one extra link that connects the point mass and the upper end of the linear spring. The link is perpendicular to the spring, and its length is

parametrized by a new intrinsic parameter d. The positive and negative offset values of d indicate that the spring is ahead and behind the point mass, as shown in Fig. 1(b) and 1(c), respectively. When d changes, the distance between the body point mass and the lower end of the spring in the leg's natural configurations is set to be the same, so the overall size of the model size is maintained. The functionality and dynamics of the robot leg can be differentiated (e.g. more braking or more thrust) when the front, middle, and hind legs of the robot utilize different model legs, as shown in Fig. 1 (a)–(c).

(ii) The model has leg point mass (m_{leg}) located at a fixed distance (l_{leg}) from the lower end of the spring (i.e. ground contact point). Because the lower half of the empirical robot leg was much heavier than the upper half, the fixed l_{leg} was reasonable. The added leg mass provides a better mapping from the template, the abstract model, to the anchor, the empirical robot.

(iii) The model has external torque (τ), which drives the legs similar to the setup of many non-conservative SLIP-like models [11].

Based on this design, the leg model with positive d generates greater thrusting force during stance phase; in contrast, the model with negative d provides greater braking force. Therefore, when the hexapod robot utilized the differentiated legs, as shown in Fig. 1(d), the animal-like motion pattern in which more braking in the front leg and more acceleration in the hind leg can be regenerated in the robot. The leg model is hereafter referred to as the eccentric-SLIP (eSLIP) model.

B. Equations of motion of the eSLIP model

The equations of motion (EOM) of the model in stance phase were derived using the Lagrangian method as follows:

$$\frac{d}{dt}\left(\frac{\partial Lag}{\partial \dot{q}_l}\right) - \left(\frac{\partial Lag}{\partial q_i}\right) = \tau \tag{1}$$

where the symbols Lag, q, and τ represent the Lagrangian, the generalized coordinates, and the non-conservative generalized forces/torques, respectively. The model was parametrized by two generalized coordinates, $q = [l, \phi]^T$, that represented the leg configuration, as shown in Fig. 1(b) and 1(c). Two generalized forces/torques were defined as $\tau = [0, \tau_\phi]^T$, where the motor torque rotates the leg. Therefore, the Lagrangian (Lag) can be expressed as follows:

$$\begin{aligned} Lag(q,\dot{q}) = T - V = \frac{1}{2}m(\dot{x}^2 + \dot{z}^2) + \frac{1}{2}m_{leg}(\dot{x}_{leg}^2 + \dot{z}_{leg}^2) \\ -\frac{1}{2}k(l_0 - l)^2 - mgz - m_{leg}gz_{leg} \end{aligned} \tag{2}$$

where l_0, T, and V represent the natural leg length, kinetic energy, and potential energy, respectively. The symbols (x,z) and (x_{leg}, z_{leg}) are the fore, aft, and vertical displacements of the point mass and the leg point mass, respectively. Next, the displacements of the point mass and the leg point mass, respectively, can be written as functions of generalized coordinates:

$$\begin{cases} x = l\sin\phi - d\cos\phi \\ z = l\cos\phi + d\sin\phi \end{cases} \tag{3}$$

and

$$\begin{cases} x_{leg} = l_{leg}\sin\phi \\ z_{leg} = l_{leg}\cos\phi \end{cases} \tag{4}$$

By substituting (3) and (4) into (2), the energies can be written as follows:

$$T = \frac{1}{2}m[\dot{l}^2 + \dot{\phi}^2(l^2 + d^2) + 2d\dot{l}\dot{\phi}] + \frac{1}{2}m_{leg}(l_{leg}^2\dot{\phi}^2) \tag{5}$$

$$V = mg(l\cos\phi + d\sin\phi) + m_{leg}g(l_{leg}\cos\phi) + \frac{1}{2}k(l_0 - l)^2 \tag{6}$$

The EOMs of the eSLIP model are written as follows:

$$\begin{aligned} \left(l^2 + \frac{m_{leg}}{m}l_{leg}^2\right)\ddot{l} = \dot{\phi}^2 l\left(l^2 + d^2 + \frac{m_{leg}}{m}l_{leg}^2\right) + 2\dot{l}\dot{\phi}ld \\ -g[\left(l^2 + \frac{m_{leg}}{m}l_{leg}^2\right)\cos\phi + \left(ld + \frac{m_{leg}}{m}l_{leg}^2\right)\sin\phi] \\ +\frac{k}{m}(l_0 - l)\left(l^2 + d^2 + \frac{m_{leg}}{m}l_{leg}^2\right) - \frac{\tau_\phi d}{m} \end{aligned} \tag{7}$$

$$\begin{aligned} \left(l^2 + \frac{m_{leg}}{m}l_{leg}^2\right)\ddot{\phi} = -2\dot{l}\dot{\phi}l + g\left(l\sin\phi + \frac{m_{leg}}{m}l_{leg}\sin\phi\right) \\ -\dot{\phi}^2 ld - \frac{kd}{m}(l_0 - l) + \frac{\tau_\phi}{m} \end{aligned} \tag{8}$$

In the given touchdown states (v, α, β), the motion of the eSLIP model in stance phase can be numerically computed and simulated. When the leg spring returns to its original length (l_0), the model lifts and enters the flight phase. According to the conservation of momentum, the liftoff velocity of the model (v^+) is written as follows:

$$v^+ = \frac{mv^- + m_{leg}v_{leg}^-}{m + m_{leg}} \tag{9}$$

The motion of the eSLIP model in the flight phase can be modeled as a ballistic flight, and the leg is reposed in waiting for the next touchdown. If the model runs stably, the model performs alternating stance phases and flight phases. If the liftoff velocity of the model is not in the forward and upward direction, the model may bounce back or fall. Both conditions will be considered failures, and the simulation is ceased.

III. Robot Motion Using the eSLIP Model as the Template

The use of the eSLIP model as the template for the robot as the anchor has two purposes: one is to initiate the stable running behavior of the robot based on the running dynamics of the model; the other is to differentiate leg braking and acceleration functionality using different offset parameters (d) of the eSLIP model.

A. Trajectory planning of the robot leg using the model

The stable running of the robot is initiated using stable running of the model. Previously, we utilized the R-SLIP model as the template for initiating the stable running of the RHex-style robot, which has half-circular legs [10]. In that work, the fixed-point motion of the R-SLIP model was found, and then its motion was utilized to set the robot leg trajectory as the reference. In other words, the robot was intended to run according to the passive dynamics of the model.

Here, the similar strategy of leg trajectory planning was deployed to initiate eSLIP-based running in the robot. To simplify the planning process, some assumptions were made. First, the leg mass (m_{leg}) was ignored because it was relatively small compared to the body mass (m). Second, running according to the passive dynamics of the model was desired, so the external torque (τ) in this stage was assumed to be zero. Empirically, the robot leg had mass, so torque was required to drive the leg, especially when the leg swung in the aerial phase. When the robot in the stance phase ran at the passive dynamics of the model, the required torque could be reduced to merely compensate for the loss. After the modification, the only difference between the eSLIP model and the SLIP model was the offset distance (d).

The EOMs of the simplified model were derived based on the EOMs of the eSLIP model shown in (7) and (8) by removing the leg mass and torque terms. Because the representation using (l, ϕ) is difficult to link to the effect of the offset parameter d, a new set of generalized coordinates $q = [L, \theta]^T$ was introduced, which defined length and angle from the point mass to the ground contact position, as shown in Fig. 1(b). The relations between two sets of coordinates are as follows:

$$l = \sqrt{L^2 - d^2} \tag{10}$$

$$\phi = \theta + \sin^{-1}\frac{d}{L} \tag{11}$$

The energies T and V can be rewritten as

$$T = \frac{1}{2}m(\dot{L}^2 + \dot{\theta}^2 L^2) \tag{12}$$

$$V = \frac{1}{2}mL\cos\theta + \frac{1}{2}k(l_0 - \sqrt{L^2 - d^2})^2 \tag{13}$$

Thus, the EOMs of the simplified eSLIP model can be derived as

$$\ddot{L} = L\dot{\theta}^2 - g\cos\theta + \frac{k}{m}\frac{L}{\sqrt{L^2 - d^2}}(l_0 - \sqrt{L^2 - d^2}) \tag{14}$$

$$\ddot{\theta} = \frac{1}{L}(g\sin\theta - 2\dot{L}\dot{\theta}) \tag{15}$$

Equations (14) and (15) reveal an important fact. Because the parameter d appears in the form d^2, two models with the same intrinsic parameters (m, l, and k) and offset magnitude $|d|$ but different offset directions perform the same body dynamics (i.e. the same $L(t)$ and $\theta(t)$) given the same touchdown states (L, θ, $\dot{L}$ and $\dot{\theta}$).

The characteristics of the simplified model described in the immediately previous paragraph allow the leg trajectory of the robot to be planned using the simplified model without complicated robot models, such as the full-body model and the planar rigid-body model. In robots with simplified eSLIP legs, where $+d$ and $-d$ are the hind leg and the front leg, respectively, if the robot touches down horizontally (i.e. the front and hind legs have the same touchdown states), as shown in Fig. 1(d), the robot maintains zero body pitch during the stance phase. This phenomenon is further extended to the following useful strategy: if the stable running motion (i.e. the fixed point) of the simplified model is found, the motion is directly utilized to set the robot leg trajectory, and the robot can perform a stable running motion without any pitch variation.

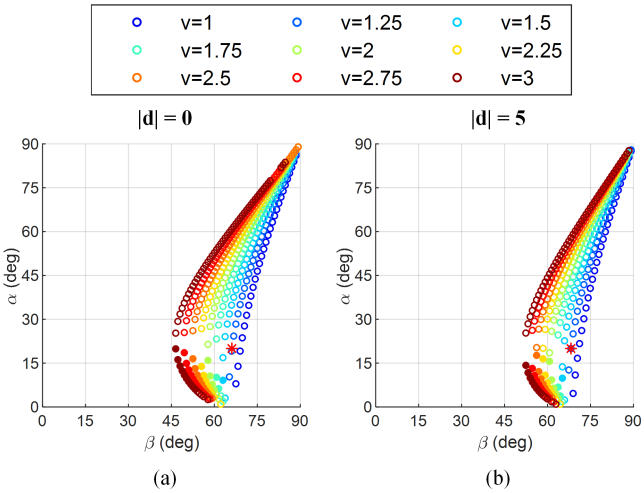

Fig. 2. The fixed-point distribution of the models without offset ($|d|$ = 0) and with offset ($|d|$ = 5). The solid and hollow dots represent stable and unstable fixed points, respectively. The red stars shown in both figures represent the fixed point (v = 1.25 m/s and α = 20°) adopted in the experiments

TABLE I

THE PARAMETERS OF THE MODEL AND THE ROBOT

Symbol	Property	Quantity
m	Mass of the robot with aluminum legs	7.7 kg
	Mass of the robot with steel legs	8.5 kg
m_{leg}	Mass of the aluminum leg	0.225 kg
	Mass of the steel leg	0.340 kg
k	Torsion spring constant	2500 N/m
L	Distance from the point mass to the ground contact point	0.14 m
l_o	Spring natural length $\|d\|$ = 0 cm	0.14 m
	Spring natural length $\|d\|$ = 5 cm	0.1308 m
l_{leg}	Distance from the leg mass to the ground contact point	0.7*l_o m

The Poincaré return map was utilized to analyze the stability of the simplified model and to explore adequate touchdown events, which were selected as the Poincaré section. The landing angle (β) is assumed to be fixed when the model runs in a periodic and stable motion. In this case, the touchdown speed (v) is also fixed because the model is conservative. Thus, the touchdown angle (α) is the only parameter to be analyzed, and the return map is one dimensional. The touchdown states are regarded as the fixed point if the touchdown angle (α) satisfies the following

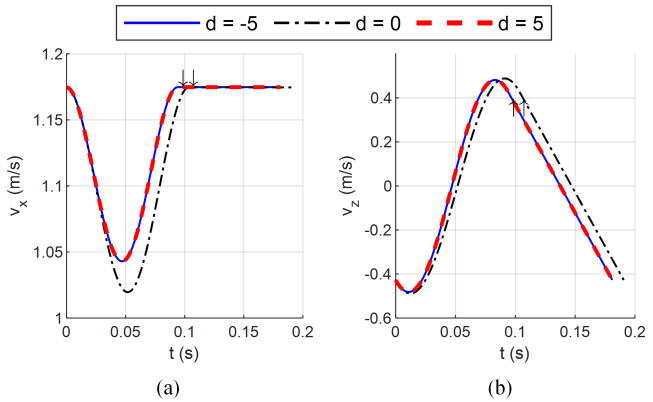

Fig. 3. Fore/aft (a) and vertical (b) velocity of the simplified eSLIP model with various offsets. The fixed points used here are shown as the red stars in Fig. 2, where the touchdown states are v = 1.25m/s, α = 20°. The arrows show the time at which the liftoff of the legs occurred.

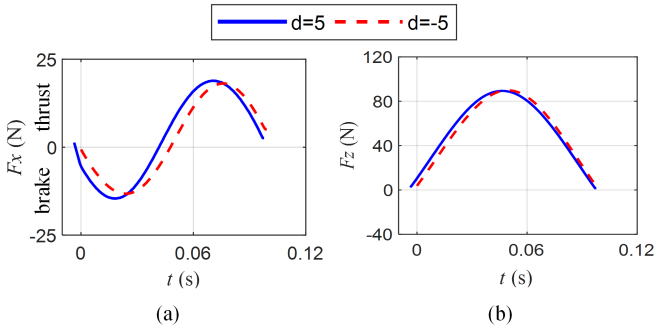

Fig. 4. The fore/aft and vertical ground reaction forces of the eSLIP model while the model runs at the fixed point with touchdown states v = 1.25m/s, α = 20°.

criteria:

$$\alpha_{n+1} = \alpha_n = \alpha^* \tag{16}$$

Using the EOMs of the model shown in (14) and (15), the distribution of stable and unstable fixed points of the simplified model with different touchdown speeds and touchdown angles is derived. In the example shown in Fig. 2, the parameters of the model were selected to match those of the empirical robot (Table I). The landing angle (β) was represented as θ coordinates. Figure 2 reveals that the fixed-point distribution of the model with and without an offset has a similar distribution trend, yet the precise combination of the touchdown states differs; the model with offset d has a smaller variation in the landing angle. Figure 3 shows plots of the point-mass velocity of the model with different offset values and a specific set of touchdown states. This particular fixed-point is also marked in Fig. 2. As shown in Fig. 3, the models with the same offset magnitude $|d|$ but different offset directions perform the same dynamic behavior. In the empirical implementation, the robot utilized the motion of one of the fixed points of the model as the reference, where the model's passive dynamic motion $\theta(t)$ served as the reference trajectory of the robot's legs $\theta_{fp}(t)$.

The middle leg of the robot utilized the leg of the model

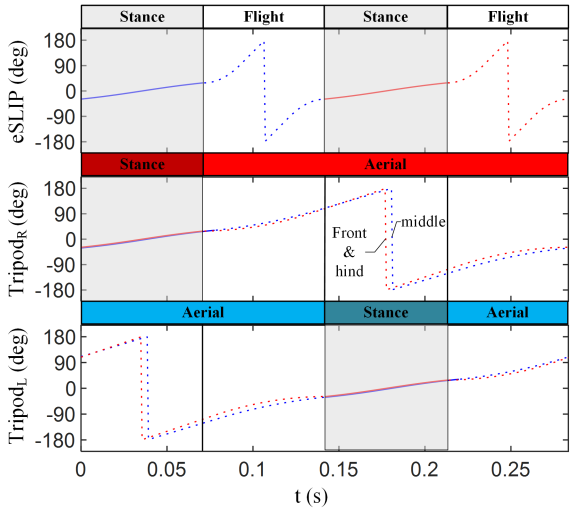

Fig. 5. Leg trajectories of the eSLIP model and the robot. The robot utilizes alternating tripod gaits, so two sets of leg trajectories are presented.

without offset, as shown in Fig. 1(d). Its natural length was set as follows:

$$d^2 + {l_0}^2 = constant \tag{17}$$

Therefore, the front, middle, and hind legs had the same hip-to-foot distance. The middle leg used the same leg trajectory as the front and hind legs, so all legs of the robot touched down simultaneously.

Considering motion in the sagittal plane, the robot itself had intrinsic rigid-body dynamics (i.e. one extra rotational DOF). However, the proposed leg trajectory planning method was aimed to prevent the rotational motion of the robot, so the motion was planned using a simple reduced-order point with only the point mass. Although the rigid-body model may better predict the robot motion, it also significantly increases the complexity of finding the adequate operation point (i.e. the fixed point) and leg trajectory [24]. The proposed strategy provides a simple yet useful approximation for use in designing the leg trajectory of the robot.

B. Ground reaction force pattern of the robot estimated using the model

After the reference leg trajectory of the robot was designed, the force interaction between the ground and the legs was simulated to validate whether the front and hind legs with different offset directions could generate the expected asymmetric brake-acceleration force pattern in the fore and aft directions. Empirically, the robot utilized simple proportional-derivative position control to drive the rotational state of the legs (θ), same strategy as report in [11], so the model's external torque input could be written as follows:

$$\tau = K_p(\theta_{fp} - \theta) + K_D(\dot{\theta_{fp}} - \dot{\theta}) \tag{18}$$

Figure 4 shows the ground reaction force patterns of the model with the same offset magnitude but different directions: d = *5* and d = *-5*. The front leg (i.e. d = *-5*) had a longer braking period than the hind leg had (i.e. d =

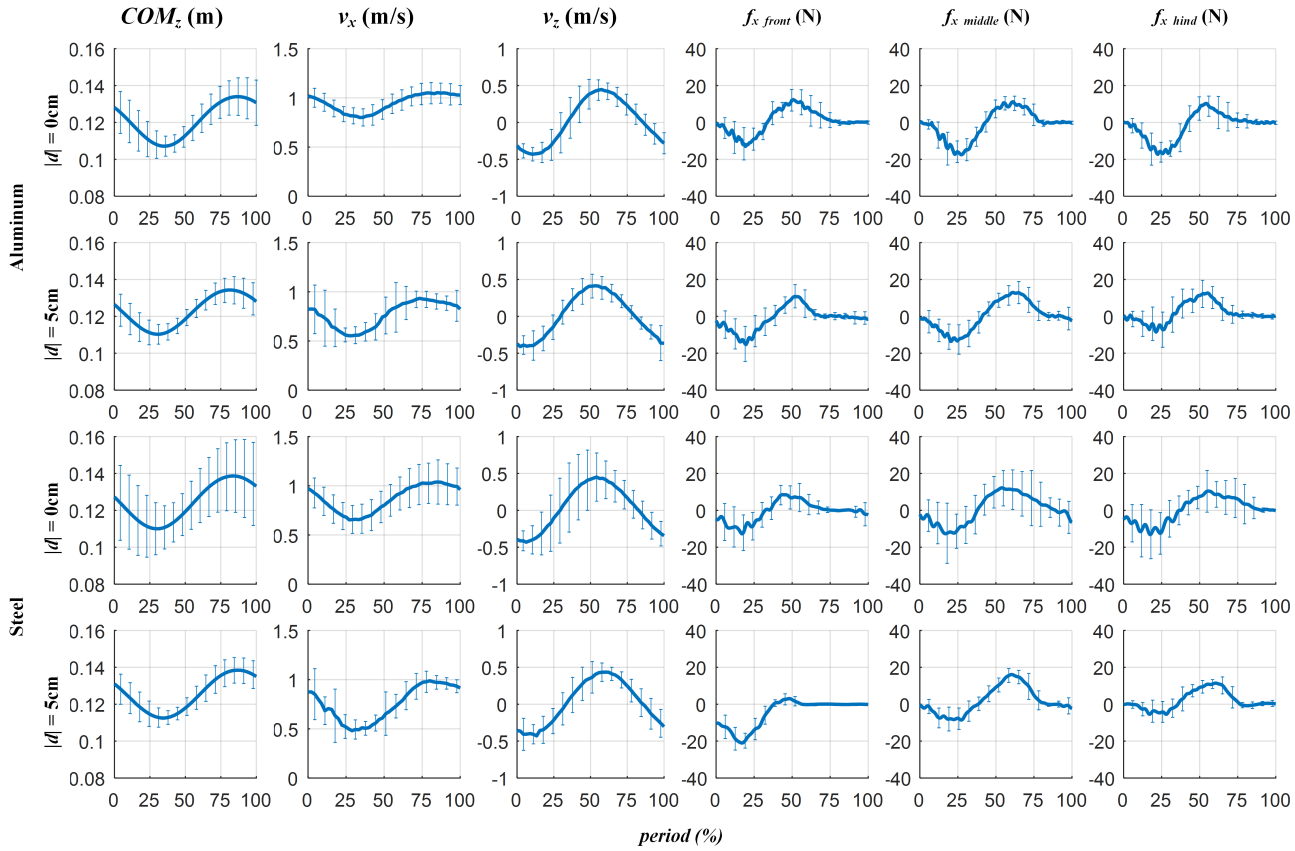

Fig. 6. The sagittal-plane motion states of the robot. The robots with and without offset legs are marked $|d| = 5\ cm$ and $|d| = 0\ cm$, respectively. The upper two rows and bottom two rows represent the data on the robot using aluminum and steel in the lower leg, respectively. The motion states include the vertical COM displacement (COM_z), the COM fore/aft and vertical velocity (v_x and v_z), and the fore/aft ground reaction force of the front, middle, and hind legs ($f_{x\,front}$, $f_{x\,middle}$, $f_{x\,hind}$), respectively. The horizontal axis represents the normalized period. The solid curves and vertical bars represent the mean and standard deviation (std) of the robot's states, respectively.

5). To quantitatively represent the results, the mean force was computed, in which the sampling forces of one period were summed and then divided by the number of samples. The mean forces of the front and hind legs were 2.16 N and 2.60 N, respectively, which indicates that the hind leg generated more thrust than the front leg did.

IV. The Robot and the Experiments

A. Experimental setup

The RHex-style robot shown in Fig. 1(e) served as the experimental platform to evaluate the eSLIP-based strategy proposed in this work, including the differential leg design and leg trajectory planning strategy. The robot was called RHex-style in the sense that each leg only had one active rotational DOF in the sagittal plane. Instead of using half-circular compliant materials as the leg, this robot had an eSLIP-like leg design, as shown in Fig. 1(e). The robot had a real-time embedded control system (sbRIO-9602, National Instruments) running at 400 MHz and an integrated FPGA that served as the main computation power in the robot. The robot had one active rotational DOF per leg, and each leg was driven by a DC motor with positional capability.

The eSLIP leg was custom-made and composed of aluminum housing, a linear spring, a linear bearing, a lower leg rod, and a rubber foot, as shown in Fig. 1(g). Because aluminum and steel were utilized in the lower leg rod, the effect of the leg mass could be verified. The masses of the aluminum leg and the steel leg were 0.225 kg and 0.340 kg, respectively. The housing had several holes for mounting to the motor shaft, so the leg could be set at different offset values d. Because all legs needed to meet the natural length requirement shown in (17), when the offset value d changed, the length of the lower leg had to change simultaneously. The offset $|d| = 5\ cm$ was utilized, where the front and hind legs were set $d = -5\ cm$ and $d = 5\ cm$, respectively. The middle leg utilized an ordinary SLIP leg (i.e. $d = 0\ cm$). In addition, the robot without offset legs (i.e. all legs $d = 0\ cm$) was also experimentally validated to serve as the control.

When the robot ran at the selected fixed point of the model, its period of one tripod was equal to two periods of the model because the robot utilized an alternating tripod gait. The period of the stance phase of the robot was identical to that of the model, but the aerial phase was equal to one stance phase and two flight phases of the model, as shown in Fig. 5. The trajectories of the front and hind legs of the

same tripod were identical, as described in Section III, and that of the middle leg differed only slightly.

The fixed point $v = 1.25m/s$ and $\alpha = 20^\circ$ were selected as the reference touchdown states. The robot with offset legs utilized the fixed point of the eSLIP model. In contrast, the robot without offset legs utilized that of the SLIP model. Because the touchdown states were the same, the leg trajectories of both models were highly similar, which provided the basis for a fair comparison. Thus, if the robot with or without offset legs behaved differently, the leg morphology could be regarded as the key factor in this behavioral difference.

In the experiments, the robot was set to run straight on a runway seven meters in length in the ground truth measurement system (GTMS) to yield body state. The GTMS was composed of a motion capture system (nine high-speed cameras, six T20s and three V5, VICON) and three 6-axis force plates (FP4060-07, Bertec). The former was utilized to yield quantitative body motion states, including COM displacements and body orientations. The latter was utilized to obtain the ground reaction forces of the robot. Because the individual leg ground reaction force was required for the analysis, the post-process was executed to identify the leg that contacted the force plate.

B. The experimental results

Figure 6 plots the sagittal plane motion states of the robot. Consider the COM motion states shown in left three columns, the robot in all four configurations exhibits typical SLIP-like running motion—the COM seems virtually connecting to a passive spring and its goes through leg compression and release states during the stance phase, and then the system goes to flight phase. The robot behaviors were also matches those of the models, except for the fore/aft velocity. The motion patterns of the robot were similar to those of the model yet the magnitudes were less than latter owing to leg slippage. The models assume point contact without slippage but empirically it is hard for the robot to satisfy this requirement owing to the very dynamic motion (i.e. the leg rotates up to 3Hz).

The three columns from the right in Fig. 6 plot the fore/aft ground reaction forces of the robot, and the averaged fore/aft forces of each leg of the robot are listed in Table II. The force patterns of the robot with aluminum legs and without offset have less pattern variations and are close to the pattern of the SLIP model where braking and thrusting roughly take half of the period in stance phase. This indicates that the use of SLIP-like leg and SLIP fixed-point trajectory can successfully initiate the running motion of the robot. The force patterns of the robot with aluminum legs and with offset (i.e. second row) have similar behavior, yet the robot exhibited a more distinct brake/thrust pattern of the front and hind legs. The front and hind legs have averaged brake force 1.27 N and averaged thrust force 1.82 N, respectively. The peak brake and thrust force are 15.29 N and 12.67 N, respectively.

The robot with steel legs and without offset have similar brake/thrust pattern among all three legs. The larger std indicates the motion of the robot may be less stable, but the magnitudes of averaged force are all less than 0.7 N. The robot with steel legs and with offset have the most distinct brake/thrust pattern of the front and hind legs. The front and hind legs have averaged brake force 4.63 N and averaged thrust force 1.98 N, respectively. The averaged brake force of the front leg goes up to 22.05% of the peak force and the average thrust force of the hind leg becomes 17.32% of the peak force. In this case, the middle leg also helps to thrust the robot. This phenomenon matches the prediction of the eSLIP model: When the model includes leg mass, the offset configuration of the model plays a role in force pattern. The larger the leg mass, the greater the effect. The leg mass of the steel rod and the aluminum tube are 0.340 kg and 0.225 kg, respectively.

TABLE II

THE AVERAGE FORE/AFT FORCE OF THE LEGS OF THE ROBOT IN RUNNING

$\lvert d\rvert$ *(cm)*	Front (N) Mean (std)	Middle (N) Mean (std)	Hind (N) Mean (std)
		Aluminum leg	
0	0.63 (5.04)	-1.15 (4.29)	-1.95 (5.12)
5	-1.27 (5.49)	0.12 (5.34)	1.82 (5.63)
		Steel leg	
0	-0.64 (5.44)	0.52 (9.93)	0.26 (8.34)
5	-4.63 (2.56)	1.83 (4.43)	1.98 (3.42)

TABLE III

THE PITCH AND ROLL VARIATIONS OF THE ROBOT IN RUNNING

$\lvert d\rvert$ *(cm)*	Roll (deg) Mean (std)	Pitch (deg) Mean (std)
	Aluminum leg	
0	0.06 (1.88)	-0.32 (1.77)
5	-0.62 (2.22)	1.11 (1.62)
	Steel leg	
0	-0.60 (3.58)	-1.71 (3.60)
5	-0.93 (3.40)	0.23 (2.23)

Table III lists the mean and std of the pitch and roll of the robot in the running experiment. The means are mostly within 1 deg, which indicates the robot body remained horizontally during running. The table also reveals that the robot with steel leg had larger std than the robot with aluminum leg. The fast spinning legs with mass resulted in pitch and roll variations of the robot in flight phase owing to conservation of angular momentum. The larger leg mass causes the larger pitch and roll variations of the robot during motion. This unwanted effect could be damped out in the following stance phase and stabilized the robot, so the robot could perform continuous and stable running. As can be seen in Fig. 6 the left three columns, the robot with steel legs and with offset seems having better stabilization ability than the robot without offset.

V. CONCLUSION

We report on the development of a running hexapod robot whose front and hind legs have differentiated braking/thrusting force patterns like the legged animals do using

the eSLIP model. The eSLIP model extends the SLIP model by the addition of one extra bar to offset the direction of the spring force to the point mass. The eSLIP model also includes external torque and leg mass to take into account the realistic issues of the empirical robot. In this work, the model with different offset magnitudes generated different ground braking and thrusting force patterns. When the leg mass of the model was ignored, the passive dynamics of the model with the same offset magnitude but different directions had the same motion dynamics. The EOMs of the model were derived using the Lagrangian method, and these two characteristics were verified in the simulation. The eSLIP model served as the foundation for developing a running robot with leg functionality differentiation in both design and motion control.

The front and hind legs of the robot were designed to use the eSLIP leg with the same offset magnitudes but different offset directions. Because the dynamic behavior of these two eSLIP legs was the same, the robot was expected to run without pitch variations. Thus, the motion of the robot was designed using the model's passive dynamic motion (i.e. fixed-point motion) as the reference of the robot's leg motion. The Poincaré return map was utilized to select the fixed point at which the parameters of the model matched those of the robot. In addition, the robot's hardware constraints were considered.

The robot with two sets of differentiated legs made of aluminum and steel materials, respectively, was fabricated to experimentally verify the proposed strategy. The robot with identical legs was also tested, and the results of their performances were compared. The results showed that the robot was able to perform a stable model-based running motion using a simple position control of the robot leg based on the fixed point motion of the eSLIP model. There was no need to adopt tuning, learning, or further optimization. The averaged pitch and roll variations in the running robot were mainly less than 1 deg. Regarding the performance of the robot leg force differentiation, the robot with aluminum offset legs produced an averaged braking force of 1.27 N in the front leg and a thrusting force of 1.82 N in the hind leg, which were about 8.31% and 14.36% of the peak force, respectively. The robot with steel offset legs produced an averaged braking force of 4.63 N in the front leg and a thrusting force of 1.98 N in the hind leg, which were about 22.05% and 17.32% of the peak force, respectively.

Currently, we are in the process of constructing a planar model to investigate the effects of the inclusion of rigid-body dynamics. We also plan to explore the behaviors of a robot with offset legs on uneven or soft terrain to further determine the benefits of differentiated legs.

REFERENCES

[1] R. M. Alexander, *Elastic mechanisms in animal movement*, vol. 404.

[2] P. Holmes, R. J. Full, D. E. Koditschek, and J. Guckenheimer, "The dynamics of legged locomotion: Models, analyses, and challenges," *SIAM Review*, vol. 48, pp. 207–304, 2006.

[3] R. Full and D. Koditschek, "Templates and anchors: Neuromechanical hypotheses of legged locomotion on land," *The Journal of experimental biology*, vol. 202, pp. 3325–32, 01 2000.

[4] J. Y. Jun and J. E. Clark, "Effect of rolling on running performance," in *2011 IEEE International Conference on Robotics and Automation*, 2011, pp. 2009–2014.

[5] M. Ankarali and U. Saranli, "Stride-to-stride energy regulation for robust self-stability of a torque-actuated dissipative spring-mass hopper," *Chaos (Woodbury, N.Y.)*, vol. 20, p. 033121, 09 2010.

[6] Z. Shen and J. Seipel, "A fundamental mechanism of legged locomotion with hip torque and leg damping," *Bioinspiration & Biomimetics*, vol. 7, p. 046010, 09 2012.

[7] J. Seipel and P. Holmes, "A simple model for clock-actuated legged locomotion," *Regular and Chaotic Dynamics*, vol. 12, pp. 502–520, 10 2007.

[8] I. Poulakakis and J. W. Grizzle, "The spring loaded inverted pendulum as the hybrid zero dynamics of an asymmetric hopper," *IEEE Transactions on Automatic Control*, vol. 54, no. 8, pp. 1779–1793, 2009.

[9] U. Saranli, "Rhex: A simple and highly mobile hexapod robot," *The International Journal of Robotics Research*, vol. 20, pp. 616–631, 07 2001.

[10] K.-J. Huang, C.-K. Huang, and P.-C. Lin, "A simple running model with rolling contact and its role as a template for dynamic locomotion on a hexapod robot," *Bioinspiration & Biomimetics*, vol. 9, p. 046004, 10 2014.

[11] W. Lu, M. Yu, and P. Lin, "Clock-torqued rolling slip model and its application to variable-speed running in a hexapod robot," *IEEE Transactions on Robotics*, vol. 34, no. 6, pp. 1643–1650, 2018.

[12] C.-J. Hu, T.-K. Wang, C.-K. Huang, and P.-C. Lin, "A torque-actuated dissipative spring loaded inverted pendulum model with rolling contact and its application to hexapod running," *Bioinspiration Biomimetics*, vol. 14, 01 2019.

[13] W. Chen, H. Lin, Y. Lin, and P. Lin, "Turboquad: A novel leg–wheel transformable robot with smooth and fast behavioral transitions," *IEEE Transactions on Robotics*, vol. 33, no. 5, pp. 1025–1040, 2017.

[14] Y. Lin, H. Lin, and P. Lin, "Slip-model-based dynamic gait generation in a leg-wheel transformable robot with force control," *IEEE Robotics and Automation Letters*, vol. 2, no. 2, pp. 804–810, 2017.

[15] R. J. Full, R. Blickhan, and L. H. Ting, "Leg design in hexapedal runners." *The Journal of experimental biology*, vol. 158, pp. 369–90, 1991.

[16] H. Cruse, "The function of the legs in the free walking stick insect, carausius morosus," *Journal of Comparative Physiology, A: Neuroethology, Sensory, Neural, and Behavioral Physiology, 112(2), pp. 235-262*, vol. 112, 09 1976.

[17] J. Chen, A. Peattie, K. Autumn, and R. Full, "Differential leg function in a sprawled-posture quadrupedal trotter," *The Journal of experimental biology*, vol. 209, pp. 249–59, 02 2006.

[18] G. Kenneally, A. De, and D. E. Koditschek, "Design principles for a family of direct-drive legged robots," *IEEE Robotics and Automation Letters*, vol. 1, no. 2, pp. 900–907, 2016.

[19] D. J. Blackman, J. V. Nicholson, C. Ordonez, B. D. Miller, and J. E. Clark, "Gait development on Minitaur, a direct drive quadrupedal robot," in *Unmanned Systems Technology XVIII*, R. E. Karlsen, D. W. Gage, C. M. Shoemaker, and G. R. Gerhart, Eds., vol. 9837, International Society for Optics and Photonics. SPIE, 2016, pp. 141 – 155.

[20] P. M. Wensing, A. Wang, S. Seok, D. Otten, J. Lang, and S. Kim, "Proprioceptive actuator design in the mit cheetah: Impact mitigation and high-bandwidth physical interaction for dynamic legged robots," *IEEE Transactions on Robotics*, vol. 33, no. 3, pp. 509–522, 2017.

[21] J. E. Clark, J. G. Cham, S. A. Bailey, E. M. Froehlich, P. K. Nahata, R. J. Full, and M. R. Cutkosky, "Biomimetic design and fabrication of a hexapedal running robot," in *Proceedings 2001 ICRA. IEEE International Conference on Robotics and Automation (Cat. No.01CH37164)*, vol. 4, 2001, pp. 3643–3649 vol.4.

[22] J. E. Clark and M. R. Cutkosky, "The effect of leg specialization in a biomimetic hexapedal running robot," *Journal of Dynamic Systems Measurement and Control-transactions of The Asme*, vol. 128, pp. 26–35, 2006.

[23] S. Kim, "isprawl: Design and tuning for high-speed autonomous open-loop running," *The International Journal of Robotics Research*, vol. 25, pp. 903–912, 09 2006.

[24] C.-K. Huang, C.-L. Chen, C.-J. Hu, and P.-C. Lin, "Model-based bounding on a quadruped robot," *2016 IEEE International Conference on Robotics and Automation (ICRA)*, pp. 3576–3581, 2016.